Erschienen in: IEEE Journal of Photovoltaics ; 4 (2014), 1. - S. 148-153
https://dx.doi.org/10.1109/JPHOTOV.2013.2286525

High Efficiency Multi-busbar Solar Cells and Modules

Stefan Braun, Robin Nissler, Christian Ebert, Dirk Habermann, and Giso Hahn

***Abstract*—In this paper, a detailed overview of multi-busbar solar cells and modules with selective emitter, a fine line screen printed front side metallization, and full aluminum rear side are presented. The designs of three-busbar and multi-busbar solar cells and modules are compared and assessed by solar cell, module performance, and Ag metal consumption. Assembled multi-busbar solar cells and four-cell modules are compared with industrial type three-busbar solar cells and modules that demonstrate average fill factor gains of 0.6%$_{\mathrm{abs}}$ on the module level. A reduction in Ag paste consumption of about 50%$_{\mathrm{abs}}$ for the front grid is achieved using the multi-busbar front electrode design with a fine line screen printing process. An advanced front side metallization technique using an Ag seed and Ag LIP approach demonstrates the potential to further reduce Ag consumption to values as low as 32 mg/cell.**

***Index Terms*—Photovoltaic cells, semiconductor device manufacture, silicon, solar energy.**

I. Introduction

HIGHER efficiencies with lower processing costs reached by lower metal consumption of the front side metallization are prerequisites for lower costs of Si photovoltaics. An optimized solar cell design using the same equipment as already available for state-of-the-art solar cells can easily be implemented into industrial solar cell production lines. In this paper, an approach for a front side design is discussed, using more busbars than the widely used three-busbar design. The idea for such a solar cell design based on multiple wires, which interconnect the cells in a module like ribbons, but substituting the busbar at the same time, was first introduced to the market by the Canadian company Day4 Energy [1].

The starting point is to optimize the solar cell series resistance under module conditions and not for a measurement on cell level [2]. For the optimization of the front grid, a simulation program based on the two-diode model is used to sum up the series resistances of each contributor in a module, optimizing the number and geometry as well as the shading of wires needed. The simulations reveal that the advantages of the multi-busbar design originate from a reduction of effective finger length, opening up new possibilities for the front side design relating to metal consumption, and grid layout. It is demonstrated that the multi-busbar solar cell design with a screen printed front grid can increase the module efficiency by 0.2%$_{\mathrm{abs}}$ [3], and simulations predict that a reduction in the Ag consumption of 80% can be achieved using seed and plate techniques. Round wires offer the beneficial effect that reflected sunlight is partly guided to the solar cell surface. The effectively shaded area of the wires is therefore reduced [3]. This effect is also enhanced when incorporating the wire solar cell into a module because of internal back reflection on the glass/air interface.

S. Braun and G. Hahn are with the University of Konstanz, Konstanz D-78457, Germany (e-mail: stefan.braun-shirazi@uni-konstanz.de; giso.hahn@uni-konstanz.de).

R. Nissler, C. Ebert, and D. Habermann are with Gebr. Schmid GmbH&Co, Freudenstadt D-72250, Germany (e-mail: nissler.ro@schmid-group.com; ebert.ch@schmid-group.com; habermann.di@schmid-group.com).

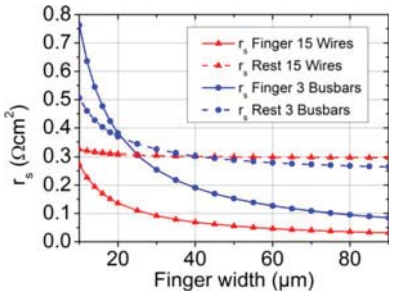

Fig. 1. Series resistance contribution plotted versus the width of a screen printed finger of a multi-busbar and a three-busbar solar cell. In the dashed lines, the remaining part of the series resistance is plotted. By adding the finger contribution to the rest, one obtains the total series resistance of the solar cells.

II. Simulation

The two-diode model is used to simulate the *IV* characteristics [4]. An Excel spreadsheet determines the series resistance [5] for both solar cell types on cell and module level and solves the two-diode model equation for each given parameter using iteration algorithms. Additionally, the optimum number of wires is calculated for each wire diameter. In addition, the optimal amount of Ag needed for a sufficient front side metallization is calculated. The outcome of the simulations is presented in Section IV.

The simulations reveal the beneficial effects of the front grid design of multi-busbar solar cells. In Fig. 1, the series resistance contribution of a screen printed Ag finger is displayed for a three-busbar and a multi-busbar solar cell with 15 wires. The assumption is made for the *IV* setup that the current is collected with 15 pins on each busbar and that the rear side of the solar cell has full contact to the metal chuck. For the multi-busbar solar cell, the current is collected on both edges by the wires, which is more realistic to the situation in a module.

In addition, the remaining part of the series resistance (contribution of rear side, base, emitter, contact to the emitter, and

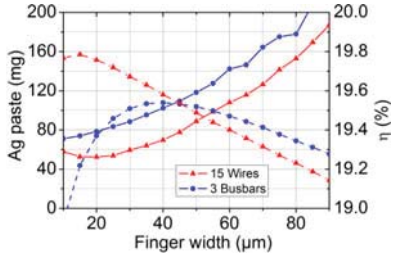

Fig. 2. Ag paste consumption (solid lines) and efficiency (dashed lines) plotted versus the finger width of screen printed solar cells.

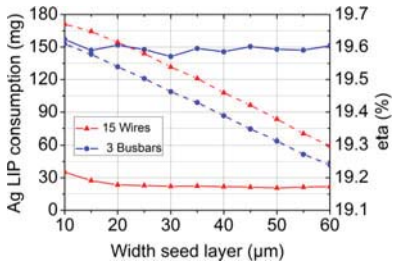

Fig. 3. Optimal amount of plated Ag needed plotted versus the seed layer width (solid lines). Efficiencies of both cell types (dashed lines).

busbars/pads) is displayed in dashed lines. By adding the remaining part to the series resistance contribution of the fingers, one obtains the total series resistance of the solar cell. A busbar width of 1.5 mm and a wire diameter of 250 μm are assumed. With decreasing finger width the series resistance contribution r_s of a Gaussian shaped finger with a height of 35 μm rises much faster for a three-busbar solar cell compared with a multi-busbar solar cell. This finger shape is more realistic compared with a rectangular finger form. Even more accurate would be to use a finger form, which also takes into account the nonuniformity of the screen printed finger [6]. In the simulation, the potential reflection of light on the grid structure was not taken into account, therefore the shading was set to 100% for the metallized area. For more accurate simulations material, roughness, and shape have to be taken into account.

The huge difference in series resistance is related to a reduced effective finger length for the multi-busbar solar cell. The shading for both solar cells is reduced with decreasing finger width. The results of the simulations indicate that the line resistance of the fingers for a multi-busbar solar cell is almost negligible. This offers possibilities not only for new metallization techniques but also for less conductive materials. Using screen printing techniques, the amount of Ag paste can be reduced significantly because the effective finger length is reduced from 25 mm for a three-busbar solar cell to only 5 mm for a solar cell with multi-busbar front grid with 15 wires and a wire diameter of 250 μm.

Taking a closer look at the Ag paste consumption and efficiency for both solar cell designs, one can observe the following. In Fig. 2, the Ag paste consumption and the efficiency are plotted versus the width of a screen printed finger with a Gaussian shaped form and an aspect ratio (finger width / finger height) of 0.5.

Both cell types benefit from a finger width reduction. The efficiency rises, however at a certain width, about 40 μm for the three-busbar and 15 μm for the multi-busbar solar cell, the efficiency drops because of the insufficient finger conductivity. This results in a higher efficiency for the multi-busbar design. The metal consumption was calculated as follows. For the three-busbar solar cell, a busbar width of 1.2 mm was assumed. For the multi-busbar solar cells, small front pads were also added in the simulation. These front pads increase the contact area to the wire and are needed to obtain a sufficient adhesion between the cell and the wire for the soldering process. These pads lead to higher Ag paste consumption and shading when going to smaller finger spacings. The size of such a pad is 500 $\times$ 500 μm^2. For each wire, one pad is needed for each finger. Depending on the finger spacing the number of pads varies.

The highest efficiency of the three-busbar solar cell is reached for an Ag paste consumption of 102 mg. The multi-busbar solar cell only needs 53 mg Ag paste to reach the highest efficiency.

For a seed and plate approach where a highly conductive metal is deposited onto a shallow seed layer, the multi-busbar design also demonstrates its advantages. The growth mode for a plated finger differs from a screen printed one. The screen printed fingers have a Gaussian shaped form and plated fingers grow during the metallization process. Its growth is two times faster in length than in height, which results in a hemicycle shape for long plating times. In Fig. 3, on the left y-axis, the optimal amount of plated Ag is plotted against the width of a seed layer indicated by solid lines. On the right y-axis, the efficiency is plotted and marked in dashed lines.

In the simulation, an Ag conductivity of 50 $\times$ 10^6 S/m is assumed for the plated base layer, which was also reported in [7]. The conductivity of the seed layer was set to zero. For the multi-busbar solar cell with 15 wires, a wire diameter of 250 μm (as the *IV*-setup) and small front pads of 500 $\times$ 500 μm^2 are assumed.

It is assumed that the growth rate of the plated Ag layer is the same on fingers, busbars, and pads. This assumption is not necessarily correct as reported in [8].

With decreasing seed layer width, the efficiency for both solar cell designs rises because the shading is reduced. At the same time, the finger spacing is reduced for decreasing width of the seed layer. The spikes in the blue line are related to a low resolution of the simulation in particularly the finger spacing which was varied in 100-μm steps. The results of the simulation indicate that the front side of a multi-busbar solar cell is sufficiently plated with 20–40 mg Ag, whereas the optimal Ag consumption for a three-busbar front grid lies in the range of 140–160 mg (optimized for efficiency, not for cost). Therefore, for a sufficient front side metallization of a multi-busbar solar cell, only a fifth of Ag is needed. In addition, a slight increase in efficiency is gained comparing the efficiencies of both cell types using the same seed layer width.

III. Experiment

In the experiment, common three-busbar solar cells are compared with multi-busbar solar cells on cell and module level. All six inch boron doped p-type semi-square Cz wafers, resistivity

2 Ω·cm, with an area of 239.12 mm^2 were alkaline textured and obtained a 55 Ω/sq. $POCl_3$ emitter diffusion. The wafers were masked by inkjet printing and etched back to about 110 Ω/sq. to form a selective emitter [9]. Edge isolation was performed by single side chemical etching. Afterwards, the wafers were cleaned and a PECVD SiN_x:H layer was deposited on the surface. The wafers were divided into three groups. Group 1 is the three-busbar front grid reference group. For the front side metallization process, 70-μm wide fingers and 1.2-mm wide busbars were printed. The width of the busbars should be reduced as much as possible to reduce the amount of Ag paste printed. On the other hand, the adhesion to the ribbon which will be soldered onto the busbar later on has also to be taken into account. The distance between the metal fingers was 2.07 mm. Around 150 mg Ag paste was used for the front side metallization with a single printing step. The rear side was screen printed with Al. Group 2 has a multi-busbar front grid design also with a full Al back surface field on the rear side. For the front side grid, a dual printing was used where only the fine line printed fingers of around 50-μm width contact the emitter structure. The amount of Ag paste used was around 40 mg, and the finger spacing for the solar cells was 1.8 mm. Group 2 obtained small Ag pads (700 × 500 μm^2) onto the conductive fingers which increase the contact area between the fingers and the wires attached later on. The amount of Ag paste used for the Ag front side pads was 30 mg. Finally, the solar cells were co-fired in a belt furnace. All solar cells were measured with a modified HALM IV flasher [10]. For contacting of the front side, a frame with 15 Cu wires with a diameter of 250 μm was used.

After this step, Group 1 and Group 2 solar cells obtained three 4-mm wide Sn stripes on the full area screen printed Al rear side, which are needed to solder the ribbons/wires on the Al rear side. The Sn was deposited via ultrasonic soldering using the TinPad technique [11]. For Group 1, the stripes were deposited in busbar direction. This leads to a continuous contact of the ribbons on the rear side. For the multi-busbar cells, the stripes were deposited perpendicular to the wire direction. In that way, each wire contacts three tin pads. In the following step, Group 1 solar cells were stringed with Cu ribbons (200 μm × 1.5 mm) on front and rear side, and the multi-busbar solar cells were interconnected with wires. For Group 2, 15 copper wires with Sn encapsulant and a diameter of 300 μm were used. Note that this wire diameter is larger than the one used for the *IV* measurement of the cells and the simulations. The increased wire diameter will decrease the series resistance further and lead to higher fill factors. Four solar cells of each group were integrated into a module. The module glass has a single sided antireflection coating. After that step, the modules were measured independently at the JRC–ESTI in Ispra (Italy). For the measurement, a square-shaped shadow mask with 318-mm edge length was used. The spacing between the solar cells was 3 mm and the space between the edges of the cells and the mask was 1.5 mm.

In a second experiment, a new front side metallization scheme was assessed. The optimal amount of Ag needed for the front side metallization was determined. These solar cells represent Group 3. A shallow Ag finger grid plus front pads, 15 pads for each finger with a dimension of 500 × 500 μm^2, was deposited. In a first step, a shallow Ag seed layer was deposited on the SiN_x:H layer over the highly doped region of the selective emitter structure using an inkjet device. After the firing process, the seed layer was strengthened using light induced Ag plating (Ag LIP). The amount of Ag deposited was varied between 5–70 mg. The solar cells were then measured with a HALM IV flasher to determine the cell parameters. The main attributes of all three groups are displayed in Table I.

TABLE I
OVERVIEW OF GROUPS

Group	Type	Rear side	Front side	Connector
G1	3-busbar	full Al BSF + TinPad	Screen Printed	200 µm x 1.5 mm
G2	multi-busbar	full Al BSF + TinPad	Screen Printed	300 µm wire
G3	multi-busbar	full Al BSF	Seed & Plate	

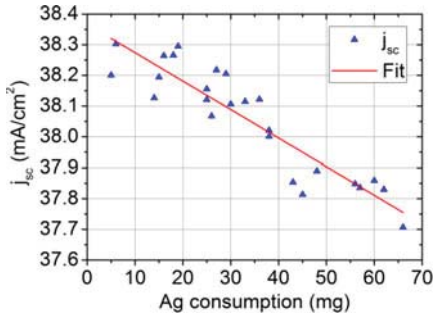

Fig. 4. Current density plotted versus the Ag consumption for solar cells with an Ag plated front grid. A reduction of Ag leads to higher current densities of the device because of reduced shading.

IV. SOLAR CELL RESULTS

For *IV* measurement, the multi-busbar solar cells are contacted with 15 wires on the front side. The diameter of these wires was 250 μm. The current was collected at the edges of the solar cells from both sides. For the seed layer deposition, 12 mg of Ag nano-particle ink was applied. The resulting seed layer width was in the range of 30–35 μm.

In Fig. 4, one can observe the linear increase of current density (indicated by the red fit curve) by reducing the amount of Ag.

This effect can be easily explained. During the plating process, Ag is uniformly deposited on the seed layer. This broadens the finger structure with increasing plating duration leading to an increased shading of the front grid.

Taking a look at Fig. 5, where the fill factor of the solar cells is plotted versus the Ag consumption, a decrease in fill factor with decreasing amount of Ag is visible. This is indicated by the red fit curve. The reduction of Ag directly leads to higher line resistances of the front side metallization, and the higher series resistance contribution affects the fill factor. As a result, the fill factor drops. On the right side of the graph, the fill factor

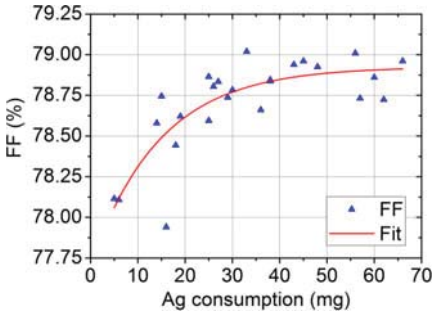

Fig. 5. Fill factor plotted versus the Ag consumption for solar cells with an Ag plated front grid. For a sufficient fill factor, the amount of Ag has to be adapted.

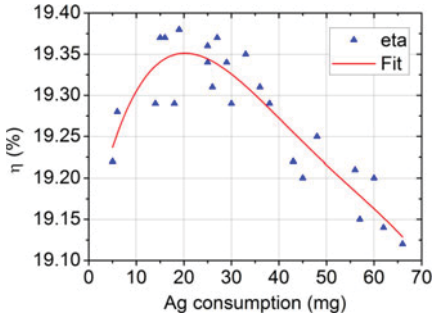

Fig. 6. The efficiency plotted versus the LIP Ag consumption for solar cells with an Ag plated front grid.

saturates because an adequate line resistance does not influence the fill factor anymore.

The efficiency plotted against the amount of plated Ag is displayed in Fig. 6. Going from 65 mg Ag to 20 mg, the efficiency rises. This effect is related to the fact that a reduced Ag consumption causes less shading of the front side, which was demonstrated in Fig. 4. The highest efficiencies can be reached in the range of 15–25 mg of plated Ag. When reducing the amount of Ag further, the efficiency drops. As a guide to the eye, a red fitting curve is also plotted in the graph.

The highest efficiencies are in the range of 19.3%–19.4% with fill factors of 78.5%–78.8%. This is a compromise between high current densities and adequate fill factors.

Even the solar cells with a sufficient Ag metallization could only reach fill factors in the range of 79%. Former experiments demonstrated higher fill factors in the range of 79.5%. This is why the authors believe that a further increase in efficiency could be reached by optimizing the processes sequence.

If we compare the results of plated Ag consumption for the experiment and the simulation, we obtain a Ag consumption of 22 mg for a seed layer with 30–35 μm in the simulation and a maximum efficiency of 20-mg Ag in the experiment. This demonstrates that the simulation is in good agreement with the experimental values.

The results of the *IV* measurement for Group 1, 2, and 3 are given in Table II. For Group 3 solar cells, the number indicates the amount of metal plated in mg. For Group 1 and 2, eight solar cells are taken to fabricate two four-cell modules.

TABLE II
IV MEASUREMENT ON CELL LEVEL

Group	V_{oc} (mV)	j_{sc} (mA/cm²)	FF (%)	eta (%)
G1-1A	641.7	38.0	79.9	19.5
G1-2A	643.1	38.0	79.8	19.5
G1-3A	642.6	38.1	79.5	19.5
G1-4A	643.1	38.0	79.8	19.5
G1-5B	642.6	38.0	79.8	19.5
G1-6B	642.7	38.0	79.8	19.5
G1-7B	642.6	38.0	79.8	19.5
G1-8B	642.9	38.1	79.7	19.5
G2-1A	644.5	37.9	79.1	19.3
G2-2A	644.5	37.9	79.5	19.5
G2-3A	644.5	38.0	79.5	19.5
G2-4A	644.9	37.9	79.7	19.5
G2-5B	643.6	37.9	79.3	19.4
G2-6B	644.4	38.0	79.6	19.4
G2-7B	643.1	38.0	79.4	19.4
G2-8B	644.7	37.9	79.6	19.5
G3-5	644.1	38.2	78.1	19.2
G3-6	644.5	38.3	78.1	19.3
G3-14	644.0	38.1	78.6	19.3
G3-15	643.9	38.2	78.7	19.4
G3-16	644.3	38.3	77.9	19.4
G3-18	642.7	38.3	78.4	19.3
G3-19	643.8	38.3	78.6	19.4
G3-25	644.9	38.2	78.6	19.3
G3-26	643.6	38.1	78.8	19.3
G3-27	642.8	38.2	78.8	19.4
G3-29	643.0	38.2	78.7	19.3
G3-30	642.4	38.1	78.8	19.3
G3-33	642.3	38.1	79.0	19.4
G3-36	643.9	38.1	78.7	19.3
G3-38	643.9	38.0	78.8	19.3
G3-43	643.3	37.9	78.9	19.2
G3-45	642.9	37.8	79.0	19.2
G3-48	643.6	37.9	78.9	19.3
G3-56	642.5	37.8	79.0	19.2
G3-57	642.6	37.8	78.7	19.2
G3-60	643.1	37.9	78.9	19.2
G3-62	643.1	37.8	78.7	19.1
G3-66	642.3	37.7	79.0	19.1

V. MODULE RESULTS

Four cells were stringed, laminated under module glass, and independently measured at the Joint Research Centre-European Solar Test Installation (JRC–ESTI). The results are presented in Table III. The edges of the modules were covered by a black polyethylene (PE) mask. The aperture area of the modules was 1011.24 cm^2 , whereas the total cell area was only 956.48 cm^2.

The modules were measured in outdoor conditions at a module temperature of 25 °C to make best use of the correct sun

TABLE III
RESULTS OF FOUR-CELL MODULES MEASURED AT JRC–ESTI

Group	V_{oc} (V)	I_{sc} (A)	j_{sc} (mA/cm²)	FF (%)	eta (%)	P_{max} (W)
G1-A	2.556	9.151	36.2	76.08	17.58	17.77
G1-B	2.556	9.127	36.1	76.31	17.61	17.80
G2-A	2.570	9.104	36.0	76.98	17.79	17.98
G2-B	2.560	9.168	36.3	76.57	17.77	17.97

spectrum. All four modules show high efficiencies in the range of 17.6–17.8%. The short circuit current densities of the three-busbar modules also shown in Table III are the current densities for the four modules calculated with the total illuminated area, not the cell area only. It is hard to determine if the slight gain in j_{sc} can be related to the round shaped wires as reported in [12]. Please note that the *IV* measurement was performed with 250-μm thick wires, whereas the modules are stringed with 300-μm wide wires.

The increased fill factor (FF) can clearly be related to the amount and thickness of wires. The cross section of all wires is 1.06 mm^2, whereas the cross section of the three ribbons is only 0.9 mm^2. An average gain of 0.6%$_{\mathrm{abs}}$ in FF can be observed. The increased fill factor can directly be related to the larger cross section of the wires. This also means that more Cu is used to increase the fill factor. A further broadening of the ribbons from 1.5 to 1.6 mm or more could also increase the amount of Cu and lower the fill factor, but would lead to higher shading. An increased ribbon height would cause more stress during the lamination process and could lead to cell breakage. In addition, the multi-busbar modules show higher open-circuit voltages. The difference of up to 14 mV can explained by the higher V_{oc} values on cell level originating from the dual printing of the front side metallization.

VI. DISCUSSION

The potential in Ag reduction for the front side metallization using a front grid with 15 wires instead of three busbars is presented in this paper. Using screen printing, an Ag reduction of more than 50% is achieved. At the same time, the solar cells demonstrate similar performance on cell level.

Changing the front side metallization to a seed and plate technique, a further Ag reduction can be seen. Twelve milligrams of Ag particle containing seed layer ink plus 20 mg Ag for LIP are sufficient for a cell performance of 19.4%. Compared with the three-busbar solar cells, the simulation predicts that an Ag reduction of 118 mg is possible.

Further process optimization offers the possibility to even increase the efficiency as the simulation reveals.

On module level efficiencies of 17.6% with a power of 17.8 W with three-busbar solar cells and an illuminated area of 1011.24 cm^2 are presented. The multi-busbar modules reach slightly higher efficiencies up to 17.8% and a module power of 18.0 W. Calculating the module power to a 60-cell module, the power of a three-busbar module would be 267 W and for a multi-busbar module a power of 270 W can be reached. A silver paste reduction of 4800 mg for such a module is possible.

VII. CONCLUSION

It was demonstrated that a multi-busbar module design shows benefits in fill factor, current density, and Ag paste consumption. Using a dual print approach, 80 mg of silver paste could be saved with the multi-busbar front design compared with the standard three-busbar front design, which is a reduction of $>$50%. With a seed and plate approach, the amount of Ag needed for the front side metallization could be further reduced to 12 mg for the seed layer and 20 mg for the plated base layer. Here, the multi-busbar cell design shows its benefits for Ag reduction.

The production of four-cell modules demonstrated the feasibility of the new design. Using only narrow fingers and small pads for the front side metallization, module efficiencies of 17.8% prove the high potential of this technology. The reference modules obtained efficiencies of 17.6%.

Because of further optimization of the cell, stringing, and lamination process, the authors believe a further increase of module efficiency is possible. A further cell optimization could be achieved using more elaborate metal deposition techniques, for example, optimized inkjet printers that can deposit narrower conduction lines or laser ablation of the SiN_x layer and direct plating [13]. The automated stringing process could be further optimized using smaller pads, which would slightly increase the current and voltage of the solar cell. A further optimized lamination process could offer thicker wire diameters. This would lead to higher fill factors and slightly lower currents, but higher efficiencies.

ACKNOWLEDGMENT

The authors would like to thank L. Mahlstaedt for help and assistance during cell processing, the TCS team for their support, and E. Salis and H. Müllejans for the module measurements at the ESTI.

REFERENCES

[1] A. Schneider, L. Rubin, and G. Rubin, "Solar cell improvement by new metallization techniques—The DAY4TM electrode concept," in *Proc. 4th World Conf. Photovoltaic Energy Conversion*, 2006, pp. 1095–1098.
[2] S. Braun, G. Micard, and G. Hahn, "Solar cell improvement by using a multi-busbar design as front electrode," *Energy Procedia*, vol. 27, pp. 227–233, 2012.
[3] S. Braun, G. Hahn, R. Nissler, C. Pönisch, and D. Habermann, "Multi-busbar solar cells and modules: High efficiencies and low silver consumption," *Energy Procedia*, vol. 38, pp. 334–339, 2013.
[4] D. S. H. Chan and J. C. H. Phang, "Analytical methods for the extraction of solar-cell single- and double-diode model parameters from I–V characteristics," *IEEE Trans. Electron Devices*, vol. 34, pp. 286–293, Feb. 1987.
[5] A. Mette, New Concepts for Front Side Metallization of Industrial Silicon Solar Cells, Ph.D. Dissertation, Dept. Eng., Univ. Freiburg, Freiburg, Germany, 2007.
[6] L. Jiang, "An improved mathematical modeling to simulate metallization screen pattern trend for silicon solar cell," in *Proc. 39th IEEE Photovoltaic Spec. Conf.*, 2013, to be published.
[7] M. Hörteis, J. Bartsch, V. Radtke, A. Filipovic, and S.W. Glunz, "Different aspects of seed layer-printed and light-induced plated front side contacts," in *Proc. 24th Eur. Photovoltaic Solar Energy Conf. Exhib.*, 2009, pp. 985–988.
[8] J. Bartsch, Advanced Front Side Metallization for Crystalline Silicon Solar Cells with Electrochemical Techniques, Dept. Eng., Dissertation Univ. Freiburg, Freiburg, Germany, 2011.
[9] H. Haverkamp, A. Dastgheib-Shirazi, B. Raabe, F. Book, and G. Hahn, "Minimizing the electrical losses on the front side: Development of a

selective emitter process from a single diffusion," in *Proc. 33rd IEEE Photovoltaic Spec. Conf.*, 2008, pp. 430–433.
[10] A. Herguth, S. Braun, G. Hahn, C. Poenisch, R. Nissler, and D. Habermann, "Towards non-permanent contacting schemes for busbar-free solar cells," in *Proc. 28th Eur. Photovoltaic Solar Energy Conf. Exhib.*, 2013, to be published.
[11] H. van Campe, S. Huber, S. Meyer, S. Reif, and J. Vietor, "Direct tin-coating of aluminum rear contact by ultrasonic soldering," in *Proc. 27th Eur. Photovoltaic Solar Energy Conf. Exhib.*, 2012, pp. 1150–1153.
[12] A.W. Blakers, "Shading losses of solar-cell metal grids," *J. Appl. Phys.*, vol. 71, pp. 5237–5241, 1992.
[13] A. Grohe, A. Knorz, M. Alemán, C. Harmel, S.W. Glunz, R. Prei, and G.W. Willeke, "Novel low temperature front side metallization scheme using selective laser ablation of anti reflection coating and electroless nickel plating," in *Proc. 21st Eur. Photovoltaic Solar Energy Conf. Exhib.*, 2006, pp. 750–753.

Stefan Braun was born in Höxter, Germany, in 1981. He received a scholarship and received the Diploma degree in physics on the investigation of multicrystalline silicon solar cells with buried contact cell structures from the University of Konstanz, Konstanz, Germany, in 2009. He is currently working toward the Ph.D. degree with the Photovoltaics Division, University of Konstanz.

His research topics include novel silicon solar cell designs and metallization techniques for industrial solar cell applications. He is the author/co-author of more than ten publications in journals and conference proceedings and holds two patents, with several patents pending.

Robin Nissler was born in Stuttgart, Germany, in 1977. He received the Diploma degree in physics from the Technical University of Munich, Munich, Germany, in 2003 and the Ph.D. degree in physics from University of Bonn, Bonn, Germany, in 2008.

He is currently with the R&D Department of the Schmid Group, Freudenstadt, Germany, where he is focusing on solar cell metallization and characterization.

Christian Ebert was born in Heidelberg, Germany, in 1981. He received the Diploma degree in physics from the University of Heidelberg in 2007.

He is currently an R&D Scientist with the Schmid Group, Freudenstadt, Germany. His work focuses on solar cell metallization for front and rear contacts, as well as solar cell contacting methods and solar module optimization.

Dirk Habermann was born in Herdecke, Germany, in 1962. He studied geoscience at Ruhr University, Bochum, Germany, where he received the Master's and Ph.D. degrees on the topic "Quantitative Cathodo-Luminescence Spectoscopy," in 1993 and 1997, respectively.

In 1998, he became an Assistant Professor of experimental physics with the Technical University Bergakademie Freiberg, Germany. In 2002 he joined the company RENA, where he became Senior Process Manager for semiconductor technology. In 2004, he left RENA and joined the Schmid Group, Freudenstadt, Germany, where he served as Director of Technology at the STN in Freudenstadt, where he was responsible for solar cell process and production technology, as well as automation technology. In 2008, he was promoted to Vice President for Research and Development at Schmid. He is the author/co-author of more than 50 publications in journals and conference proceedings and holds several patents.

Giso Hahn was born in Frankfurt am Main, Germany, in 1969. He received the Diploma degree in physics from University of Stuttgart, Stuttgart, Germany, in 1995 and the Ph.D. degree in physics from University of Konstanz, Konstanz, Germany, in 1999. He received the Venia Legendi (Habilitation) degree in experimental physics from University of Konstanz in 2005.

Since 2009, he has been an Adjunct (Apl.) Professor with the Department of Physics, University of Konstanz. He is also the Head of the Photovoltaics Division, Department of Physics, University of Konstanz, which consists of more than 50 employees. His research interests include crystalline silicon materials and solar cell process development, characterization of promising low-cost materials for photovoltaic applications, and development of adapted solar cell processes for these and other materials. He is the author/co-author of more than 230 publications in journals, books, and conference proceedings and holds several patents.

Prof. Hahn is a member of the scientific committees of various conference series (e.g., IEEE, PVSC, EU PVSEC, and SiliconPV) and workshops. His other scientific and technological achievements include reaching record efficiencies for selected crystalline silicon materials and detailed characterization of efficiency limiting crystal defects. His group is interested in transferring technologies from the laboratory stage to industry.